Unravelling the abrasion resistance of two novel meta-stable titanium alloys on the basis of multi-pass-dual-indenter tests

Li, Cong; Li, Hu; van der Zwaag, Sybrand

DOI
10.1016/j.wear.2019.203094

Publication date
2019

Document Version
Final published version

Published in
Wear

Citation (APA)
Li, C., Li, H., & van der Zwaag, S. (2019). Unravelling the abrasion resistance of two novel meta-stable titanium alloys on the basis of multi-pass-dual-indenter tests. *Wear*, *440-441*, Article 203094. https://doi.org/10.1016/j.wear.2019.203094

Wear 440–441 (2019) 203094

Contents lists available at ScienceDirect

Wear

journal homepage: http://www.elsevier.com/locate/wear

Unravelling the abrasion resistance of two novel meta-stable titanium alloys on the basis of multi-pass-dual-indenter tests

Cong Li [a,b,*], Hu Li [a], Sybrand van der Zwaag [b,c]

[a] School of Energy and Power Engineering, Changsha University of Science and Technology, Changsha, Hunan, 410114, China
[b] Novel Aerospace Materials Group, Faculty of Aerospace Engineering, Delft University of Technology, 2629HS, Delft, the Netherlands
[c] Advanced Materials Institute, School of Materials Science and Engineering, Tsinghua University, Beijing, 1000984, PR China

ARTICLE INFO

Keywords:
Abrasion resistance
Titanium alloys
Scratch test
Microstructure
Stress induced martensite

ABSTRACT

Multi-pass-dual-indenter (MPDI) scratch tests with various loading conditions were performed on two newly developed titanium alloys (Ti–10V–1Fe–3Al and Ti–10V–2Cr–3Al) to investigate their abrasion resistance under repetitive local sliding contact. A technically pure titanium sample was used as the reference. Various microstructures were established by different heat treatments, such as to turn the β-phase into a stable phase or a meta-stable phase showing Stress Induced Martensite (SIM) formation. The influence of phase evolution on the scratch resistance and corresponding failure mechanisms was unravelled. It was found that the phase morphology and fraction have a significant impact on the scratch resistance and that effect is applied load dependent. The scratch behaviour is closely related to the work hardening ability of the material surface especially at high loading conditions, while the original surface hardness is more relevant at low loading conditions. The observations definitely prove that, not withstanding the modest hardness level, a microstructure showing a combination of metastable β (trigger the stress-induced martensitic transformation) and flake α (enhancing the initial surface hardness) is the best route to improve the scratch resistance for these two titanium alloys, in particular for high load conditions.

1. Introduction

Titanium alloys, combining a low density, a high mechanical performance and an excellent corrosion resistance, are not only widely used in aeronautical and biomedical applications, but are also being seen as attractive materials for pipelines, taps, fittings and similar devices in the chemical process industry [1–3]. However, its poor sliding wear performance has become a major problem in industrial machinery applications [4].

In abrasive wear, material is displaced or detached from a solid surface by hard particles sliding with a certain velocity relatively to the surface. Depending on the type of contact, abrasion can be subdivide into two types: the two-body abrasive wear mode and three body abrasive wear mode [5]. Regardless of the wear mode, abrasion resistance is not an intrinsic property. In a tribo-system, the response of materials involves many variables such as prevailing working conditions and is very complex. During abrasion, ploughing, wedge formation, micro-cutting, micro-fatigue and micro-cracking are potential mechanisms involved in the detachment and removal of the material. Schmidt et al. studied the compound formation and wear resistance of ion implanted Ti–6Al–4V. It was found that carbon or nitrogen ion implantation could significantly reduce the oxide particle abrasion. A maximum wear resistance can be obtained by combining a high microhardness of the implanted layer and a low oxide film thickness on the surface [6]. Sawase et al. have confirmed that a TiN coating can improve the abrasion resistance of pure titanium effectively [7]. Zhu et al. demonstrated that the deposition of TiC thin films on titanium surface by ion-enhanced triode plasma CVD and a formation of carbide layer on titanium surface heated in hydrocarbon atmosphere may lead to a higher abrasion resistance [8]. Based on these studies, it can be seen that the initial material hardness is still taken as the prime indicator for predicting the abrasion resistance. However, in many cases a high initial hardness does not guarantee a good abrasion performance and it would be interesting to examine the roles of other mechanical properties, microstructure and composition in determining wear resistance. These relationships may lead to a better insight into the mechanisms involved, and hence the possibility of better alloy design. Some studies suggested that multi-phase steels with a relatively lower hardness may possess an

* Corresponding author. School of Energy and Power Engineering, Changsha University of Science and Technology, Changsha, Hunan, 410114, China.
E-mail address: liconghntu@126.com (C. Li).

https://doi.org/10.1016/j.wear.2019.203094
Received 28 April 2019; Received in revised form 18 September 2019; Accepted 14 October 2019
Available online 17 October 2019

improved abrasion resistance due to their good balance of strength and ductility [9]. The transition from mild to severe wear in Ti–10V–2Fe–3Al and Ti–6Al–4V alloys, and its dependence on microstructure was investigated by Farokhzadeh et al. [10]. It was shown that the work hardening of the subsurface plays an important role in the wear resistance of the alloys. A general model shows that in addition to hardness and depending on the type of interaction, the capability of deformation or the fracture toughness of the wearing material is very important [11]. Wang et al. studied the sliding and frictional behaviour of Ti–35Nb–8Zr–5Ta and Ti–15Mo–2.8Nb–0.2Si alloys. It has been reported that abrasion, shear delamination, material transfer and mechanical alloying were the responsible mechanisms of wear. On the other hand it was also found that the surfaces of the metastable-β titanium alloys experienced a higher extent of surface deformation and material transfer to the counterpart compared to Ti–6Al–4V (α+β titanium) alloy while abrasion was the predominant surface damage mechanism in Ti–6Al–4V alloy [12]. The combined results of all investigations suggest that the initial hardness of the materials is not the only indicator for the abrasion resistance, other mechanical properties and related microstructures of the material have to be taken into account as well.

The scratch test in which a rigid indenter with fixed shape slides over a smooth material surface at a controlled applied load and speed, simulates the abrasion process and offers, in principle, the possibility to rank the wear resistance of metallic materials of different composition and microstructure. Most commonly the scratch tests are carried out on fresh or un-deformed surfaces, which are in a very different state than the surfaces formed in an actual abrasion process, which have undergone continuous deformation and work hardening at the surface and the sub-surface. As demonstrated in Refs. [13–15], using the conventional scratch test protocol starting with a pristine surface in order to forecast the abrasion mechanism in real applications will cause severe deviations and lead to a misprediction of the abrasive resistance. However, up to now, in all reported scratch experiments performed on titanium alloys, only the conventional protocol involving a pristine starting surface and the use of only one indenter has been used [16,17].

In the present study, a new multi-pass-dual-indenter scratch test method developed by Xu et al. [18] to better mimic the real abrasion conditions is applied. A large indenter is used to conduct a multi-pass scratch pre-test to produce a wide pre-scratch with different level of work hardening, and then a small indenter is employed to evaluate the wear behaviour of the deformed surface in the wear track. This test method can not only detects the damage formation during the actual scratching process, but also clarify the interaction between the damage and the subsurface damage caused by the previous local plastic deformation.

It is generally accepted that metastable grade of β titanium alloys may undergo formation of Stress Induced Martensite (SIM) upon the application of a load. Control of this mechanism could provide a new route to the optimization of the load bearing capabilities of titanium alloys. Earlier transformation plasticity studies in Ti–10V–2Fe–3Al alloy have shown that the SIM formation can indeed result in an improved balance of strength and ductility [19]. Inspired by this, two novel multi-phase titanium alloys, Ti–10V–1Fe–3Al and Ti–10V–2Cr–3Al, with a wide range of microstructural features and different work hardening rates as a result of the occurrence or absence of SIM formation are designed. The main criteria considered for designing new alloy compositions with a (quantified) stability of in the 100% β state are the martensite start temperature Ms and the molybdenum equivalency value [20]. The abrasion resistance of various microstructures for low and high contact load conditions is revealed by carrying out the new scratch test with different pre-scratching loads. The worn scar and the evolution of subsurface area are investigated. The damage mechanisms for the different test conditions are analysed.

2. Experimental details

2.1. Materials

Two new multiphase titanium alloys (Ti–10V–1Fe–3Al and Ti–10V–2Cr–3Al) [15] with different mechanical properties were prepared at the Institute of Metal Research, Chinese Academy of Science. Each alloy weighing about 5 kg was obtained in a forged condition. The β-transus temperature of the material in its initial state was measured by dilatometry. The measured values of β-transus of Ti–10V–1Fe–3Al and Ti–10V–2Cr–3Al alloys are about 830 °C ± 5 °C and 810 °C ± 5 °C, respectively [15]. Their chemical compositions are shown in Table 1. The corresponding initial microstructures are shown in Fig. 1 [20]. The as-received microstructure of Ti–10V–1Fe–3Al alloy shows a mixture of irregular α phase with relatively low volume fraction (Fig. 1(a)). Ti–10V–2Cr–3Al alloy possesses very fine α phase with high volume fraction (Fig. 1(b)).

Using electrical discharge machining (EDM), rectangular samples of 10 mm length, 6 mm width and 4 mm thickness were prepared. Before conducting any further experiments, the thin oxide layers formed during EDM were eliminated by careful mechanical polishing. Samples were heat treated (single step and multi step) at different temperatures in a Nabertherm furnace filled with argon gas, and then quenched to room temperature with water. Table 2 summarizes the details of heat treatment conditions. Annealed samples were embedded in a cold-setting resin and prepared according to the standard Metallographic Preparation method. Standard Kroll's reagent (3 ml HF + 6 ml HNO_3 + 100 ml H_2O) was used to display various phases in two alloys. An Leica LF7M38 optical microscope was used to determine their microstructures.

2.2. Scratching test and hardness test

A CSM micro-scratch tester was employed for the scratch test. Two spherical diamond Rock-well indenters with different tip radius and cone angle were used in the experiment: one is a large indenter (J-191) with a tip radius of 100 μm and a cone angle of 120°, the other is a small indenter (SM-A15), with a tip radius of 5 μm, and a cone angle of 60°. Two testing modes with conditions as shown in Table 3 were used. For mode 1 testing, the small indenter slides directly on the initial (polished) surface. For mode 2 (MPDI) testing, the large indenter first is made to slide 10 times on the surface of the material (always in the same direction and the same load), and a long scratch of 4 mm length is formed. Then a small indenter is used to slide 2 mm long right in the centre of the large pre-scratch. The sliding speeds of the large and small indenters are 0.2 mm/s and 0.05 mm/s, respectively. All sliding tests are carried out in the same direction. The load on the large indenter was varied between 2 and 20 N while the load on the small indenter was kept constant at 0.3 N. Each experiment was repeated three times to ascertain the reproducibility of the data.

Fig. 2 illustrates a schematic drawing of the scratch track. The area surrounded by the yellow dotted lines refers to the pre-scratch track created by the large indenter. The scratch produced by the small indenter is located at the middle bottom of the large pre-scratch and correspond to the area marked by red dotted lines. The scratch depth drawn in this paper refers to the penetration depth produced by the small indenter with respect to the bottom of the wear track generated by the large indenter. After the scratch tests, the worn surfaces were analysed by a high resolution JEOL scanning electron microscopy operated at 5 kV. The Vickers hardness tester for a load of 2 N was used to determine the microhardness of the original surface of the sample, and per condition the data of 10 independent hardness measurements were averaged. The thin foils required for the TEM observations were prepared by a standard polishing procedure and a twin-jet electron-polishing technique using a solution of 21 vol% perchloric acid, 50 vol% methanol and 29 vol% n-butyl alcohol at −25 °C.

Table 1
The chemical compositions of the fabricated new alloys (in wt%).

	V	Fe	Cr	Al	O	C	N	Ti
Ti–10V–1Fe–3Al	9.97	0.97	–	3.02	0.11	0.051	0.014	Bal.
Ti–10V–2Cr–3Al	10.6	–	2.18	0.97	0.1	0.05	0.013	Bal.

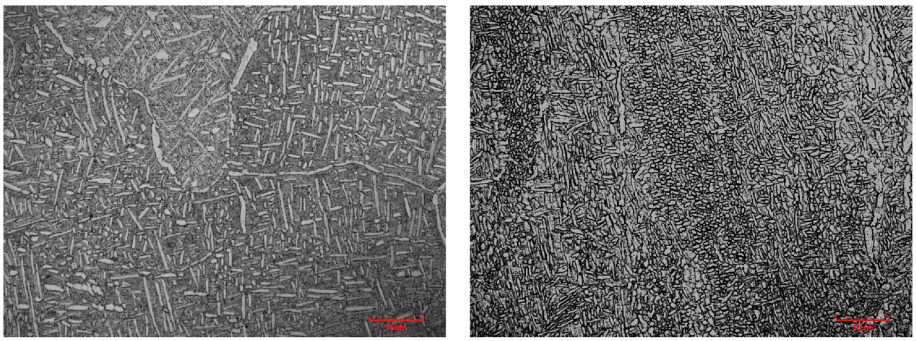

(a) (b)

Fig. 1. Microstructure of as-received condition (a) Ti–10V–1Fe–3Al, (b) Ti–10V–2Cr–3Al (scale bar =15 μm) [20].

Table 2
Performed heat treatments for two alloys.

Heat treatment	Ti–10V–1Fe–3Al	Ti–10V–2Cr–3Al
	As-received condition	As-received condition
α+β solution treatments	700 °C/15min 775°C/15min 775°C/60min 775°C/120min	700 °C/15min 775°C/15min 775°C/60min 775°C/120min
β or β +(α+β) solution treatments	900°C/15min 900°C/15min + 700°C/2min 900°C/15min + 700°C/5min 900°C/15min + 700°C/7min 900°C/15min + 700°C/10min 900 °C/15min + 700 °C/15min	900°C/15min 900°C/15min + 700°C/5min 900°C/15min + 700°C/15min 900°C/15min + 700°C/25min 900°C/15min + 700°C/35min 900 °C/15min + 700 °C/45min
β solution + aging	900 °C/15min + Quenching+400 °C/15min 900 °C/15min + Quenching+550 °C/15min 900 °C/15min + Quenching+700 °C/15min	900 °C/15min + Quenching+400 °C/15min 900 °C/15min + Quenching+550 °C/15min 900 °C/15min + Quenching+700 °C/15min

Note: Heat treatments leading to a meta-stable β phase are marked in bold.

Table 3
Test conditions of different scratch modes.

Scratch modes	Test conditions of large indenter	Test conditions of small indenter
Mode1	NA	Single pass with constant load of 0.3 N
Mode2	Multi-pass with 1 N,5 N,10 N,15 N,20 N	Single pass with constant load of 0.3 N

3. Results

Following optimal recipes from an earlier study on these alloys aimed to create different microstructures containing either stable or metastable β phases and α phases with different morphologies [20], three sets of heat treatments have been used:

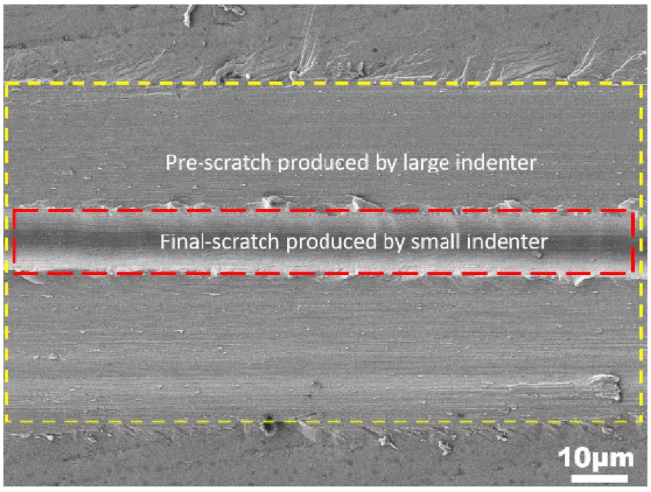

Fig. 2. The schematic drawing of scratch tracks.

(1) As received condition and α+β solution treatments
(2) β solution treatments and β + (α+β) solution treatments
(3) Aging treatment

3.1. As received condition and α+β solution treatments

The below β-transus heat treatments were conducted at 700 °C for 15 min and 775 °C for 15 min, 60 min and 120 min. Fig. 3 shows the typical optical micrographs of these alloys. All of them have a microstructure consisting of a mixture of α and β phases. The primary α phases are homogeneously distributed in the β matrix. Most parts of the α phase exhibit stubby and rod shapes, discontinuous primary α phases precipitated on and along the prior β grain boundaries, in particular for the Ti–10V–1Fe–3Al alloy. With increasing solution temperature or soaking time within the α+β domain, the α laths dissolve gradually, resulting in a decreased α phase volume fraction and a larger retained β phase fraction with a gradually changing composition and changing stability. In Table 2 those heat treatments leading to a meta-stable β phase are marked in bold.

Fig. 4(a) and (b) show the scratch depth generated by the small

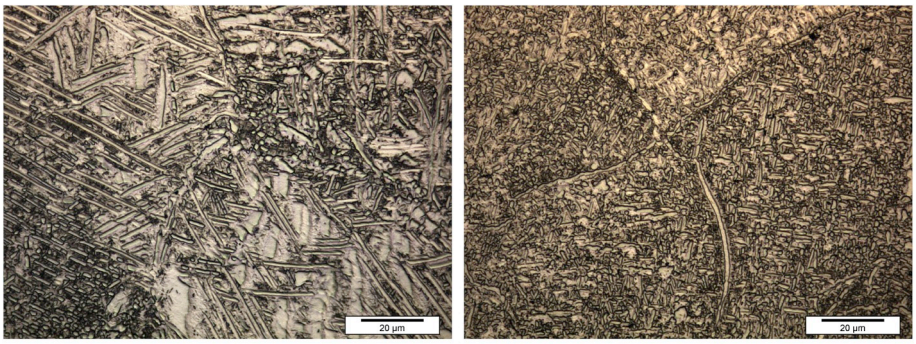

Fig. 3. Typical optical micrographs of the alloys after α+β solution treatment. (a) Ti–10V–1Fe–3Al, (b) Ti–10V–2Cr–3Al.

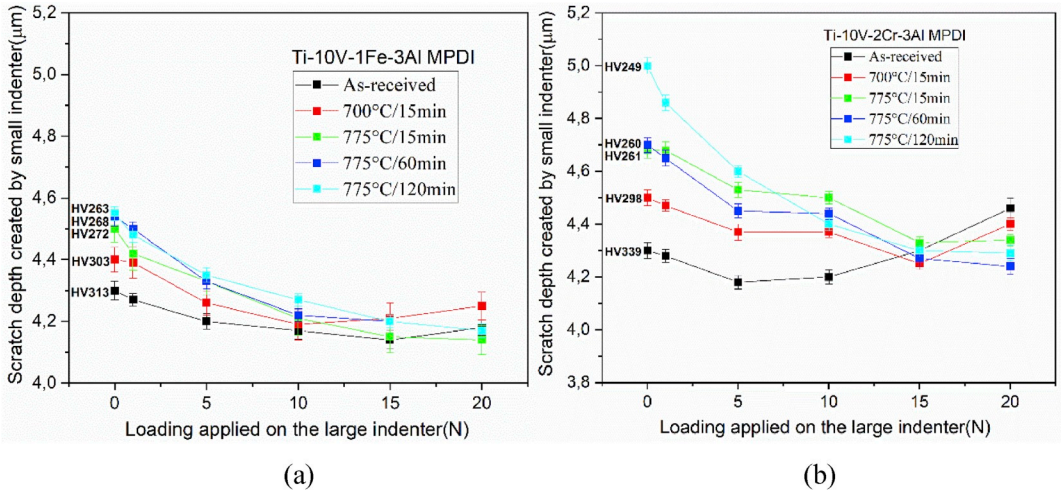

Fig. 4. The scratch depth as a function of the applied load on the large indenter for alloys after α+β solution treatment (a) Ti–10V–1Fe–3Al, (b) Ti–10V–2Cr–3Al.

indenter as a function of the applied load on the large indenter for Ti–10V–1Fe–3Al and Ti–10V–2Cr–3Al alloy respectively. The microhardness values of different samples measured by indentation are also shown. In these two graphs, the scratch depth at a load of 0 N represents the penetration depth after scratching on the original polished surface (Mode 1 test). There is a good consistency between static hardness and scratch depth of 0 N data points. While the curves for the two different alloys after the α+β solution treatments plotted in Fig. 4(a) and (b) seem somewhat different, in fact, their behaviours follow almost the same trend. The scratch depth of the original surface is relatively high. With the increase of the load on the large indenter, for all different alloys the scratch depth decreases first. The effect of surface hardening due to the pre-scratching can be well reflected by the decrease in scratch depth. For specimens in the as-received condition or the 700 °C/15 min state, with the increase of large indenter load, the scratch depth decreases until the critical load. After the critical load, the scratch depth of small indenter begins to increase again. This increase in scratch depth stands for the removal of abrasive materials and the interaction between the deformation field of the small indenter and the internal damage of the wear track. The main difference between the different conditions is the transition degree between the decreasing and increasing of scratch depth region. Furthermore, the critical load value for the as received Ti–10V–1Fe–3Al is higher than that for 700 °C/15 min testing, but the opposite holds for the Ti–10V–2Cr–3Al alloy. For samples heat treated under 775 °C from 15 min to 120 min, the scratching depth due to small indenter continues to decrease up to the maximum applied load during pre-scratching. It is worth pointing out that all samples with continuously decreasing in the scratch depth versus pre-load plots curves show the stress-induced martensitic (SIM) transformation effect [20,21].

Typical compression stress-strain curves for two samples showing SIM or not-showing SIM are presented in Fig. 5(a). It is generally accepted that the double yield point phenomenon as observed in the curve marked in red implies a stress-induced martensitic transformation, and this kind of transformation results in an improved balance of strength an ductility, although it inevitably also introduces a relatively lower yield stress. Samples showing the SIM effect exhibit a relatively high work-hardening rate as evidenced by the difference between the yield and ultimate compressive strengths. This phenomenon is well reflected in the MPDI test. In order to verify the effect of the work hardening ability on the wear resistance of the alloy, MPDI tests were also carried out on a pure titanium reference sample having a low strength and a poor work hardening ability. The results are shown in Fig. 5(b). It can be seen from the figure that the scratch depth for pure titanium decreases slightly at first and then increases rapidly with increasing pre-scratching load. The critical load of the transition point is about 1 N. Because the failure strength is relatively low, the maximum strength can also be achieved under low load. Scratch loads exceeding critical loads can lead to a severe delamination, as a result, so the additional penetration depth on new scratches increases significantly. Therefore, when comparing the behavior of the pure titanium and that of the two new multiphase alloys in which the β-phase could be brought into the metastable state, it can be concluded that the work hardening ability has a great influence on the wear resistance of the alloy under high load in

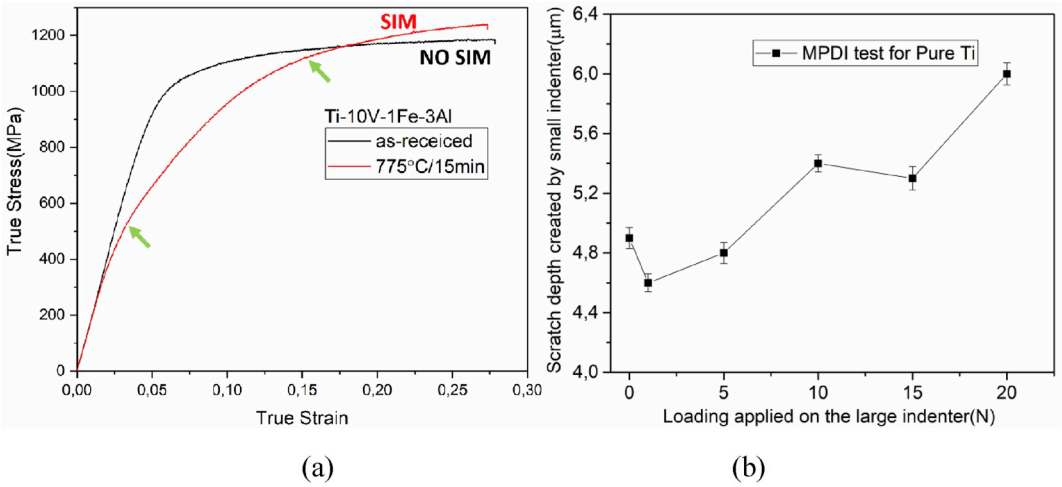

Fig. 5. (a) Typical compression stress-strain curves of Ti–10V–1Fe–3Al alloy heat treated to show or not show the SIM effect, (b) The scratch depth as a function of the applied load on the large indenter for pure titanium.

according with earlier work by others on other titanium alloys [8].

Fig. 6 shows the effect of α phase volume fraction on the work hardening ability, initial hardness and hardness of work hardening layer of the two alloys under different heat treatment conditions. It can be seen that, the work hardening ability (compressive strength-yield strength) of samples showing SIM is much stronger than that of specimens without SIM effect. With the increase of the volume fraction α phase, the work hardening ability of the alloy decreases rapidly given the reduced SIM effect. On the other hand, it can be seen from the hardness value that the pre-scratch of large indenter has an obvious strengthening effect on the sub-surface layer of the alloy. With the increase of α phase, the difference between the initial hardness and work hardening layer hardness is getting smaller which is consistent with the disappearance of SIM effect. The martensite produced by SIM transformation clearly contributes a lot to the increment of the hardness value.

3.2. *β solution treatments and β +(α+β) solution treatments*

Fig. 7(a) and (b) shows optical microstructures of β solution treated (900 °C/15 min) samples of Ti–10V–1Fe–3Al and Ti–10V–2Cr–3Al respectively. Both structures are made up of coarse β grains and a certain fraction of acicular martensite.

The purpose of β+(α+β) heat treatments is to completely get rid of the initial α particles and produce flake α instead. To achieve this aim, samples were first placed in the β phase region (900 °C/15 min) and then cooled to the α+β region (700 °C), then immersed for different time and subsequently quenched (Table 2). After such a heat treatments, flake shaped α phase was detected either in the form of isolate laths inside grains or in the form of Widmanstätten laths near the original boundaries of β grains, as shown in Fig. 8. The volume fraction of flake α phase increases with the prolongation of holding time in the α+β phase region after quenching. At the same time, when the fraction of α phase increases, the retained β phase gradually stabilizes and the β domain narrows [22].

Fig. 9(a) and (b) show the functional relationship between the scratch depth and the load applied on the large indenter, for Ti–10V–1Fe–3Al and Ti–10V–2Cr–3Al alloy respectively. It can be seen from the figure that for the samples having received the β+(α+β) solution treatment, the hardness of the samples increased compared with that of the β solid solution treated samples. Therefore, when the preloading of big indenter is 0 N (pristine surface), the scratch depth has a good correspondence with the hardness value of the sample, that is, the higher the hardness, the shallower the scratching depth. When alloys heat treated at 900 °C for 15min (β phase solution), the scratch depth decrease rapidly with increasing pre-load, and the trend remains unchanged until 20 N. With the appearance of the flaked α phase, the trend changes. The longer the holding time, the higher the ratio of α phase, the

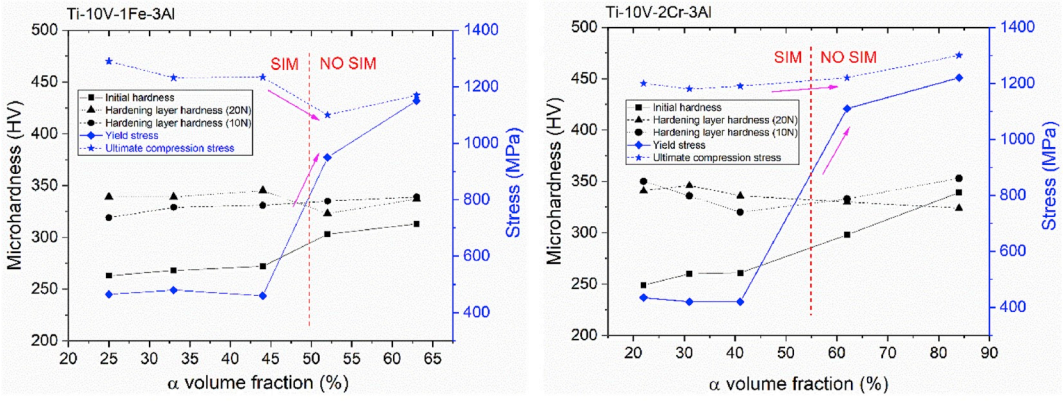

Fig. 6. Various parameters as a function of α volume fraction (a) Ti–10V–1Fe–3Al alloy solution treated in α+β phase field, (b) Ti–10V–2Cr–3Al alloy solution treated in α+β phase field.

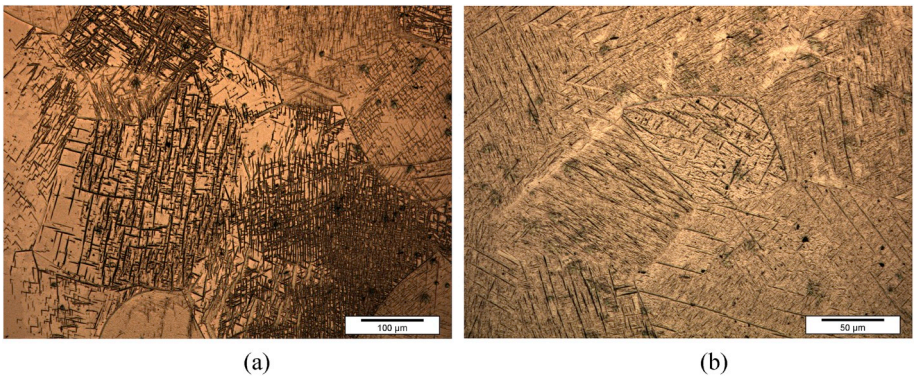

Fig. 7. Typical optical micrographs of the alloys after β solution treatment, (a) Ti–10V–1Fe–3Al, (b) Ti–10V–2Cr–3Al.

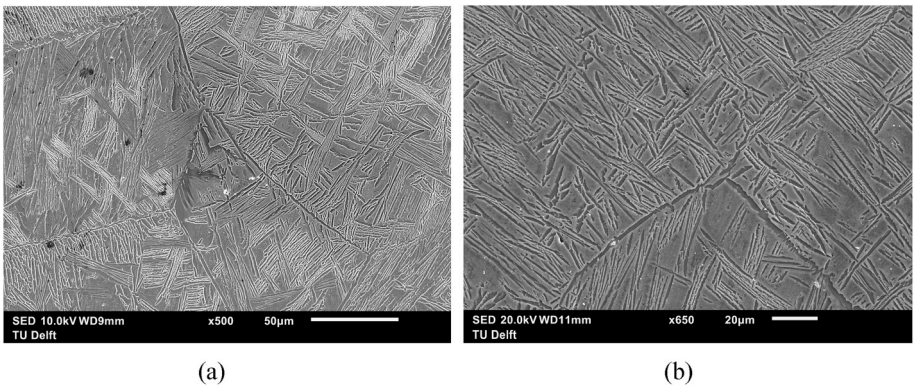

Fig. 8. Typical optical micrographs of the alloys after β +(α+β) solution treatment, (a) Ti–10V–1Fe–3Al, (b) Ti–10V–2Cr–3Al.

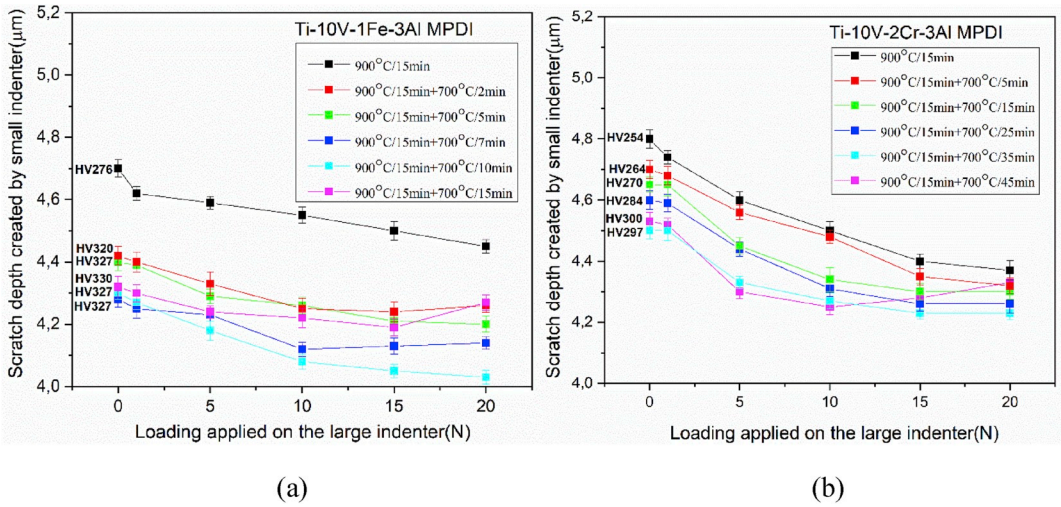

Fig. 9. The scratch depth as a function of the applied load on the large indenter for alloys after β+(α+β) solution treatment (a) Ti–10V–1Fe–3Al, (b) Ti–10V–2Cr–3Al.

more gentle the trend of curve declining. When there is an excess α phases (Ti–10V–1Fe–3Al: 900 °C/15 min + 700 °C/15 min, Ti–10V–2Cr–3Al:900 °C/15 min + 700 °C/45 min), the curve first decreases and then rises. The critical transition value of Ti–10V–1Fe–3Al alloy is higher than that of Ti–10V–2Cr–3Al alloy. Again it was found that specimens showing a continuously decreasing scratch depth-preload behavior (i.e. showed superior abrasion resistance) all show SIM behavior upon compression testing. Therefore, it can be inferred that the stress-induced martensitic transformation has a great influence on the wear resistance of these two meta-stable titanium alloys. Analyzing all data it can be concluded that Ti–10V–1Fe–3Al alloy has the best wear resistance after 900 °C/15 min + 700 °C/10 min heat treatment and Ti–10V–2Cr–3Al alloy has the best wear resistance after 900 °C/15 min + 700 °C/35 min heat treatment.

Fig. 10 shows the effect of flake α on the work hardening ability, initial hardness and hardness of work hardening layer of alloys under different β+(α+β) heat treatment conditions. Similarly, it also can be seen that the work hardening capability of the samples with SIM effect is stronger than that of samples without SIM effect, but the difference is more moderate. On the other hand, it also can be seen from the hardness

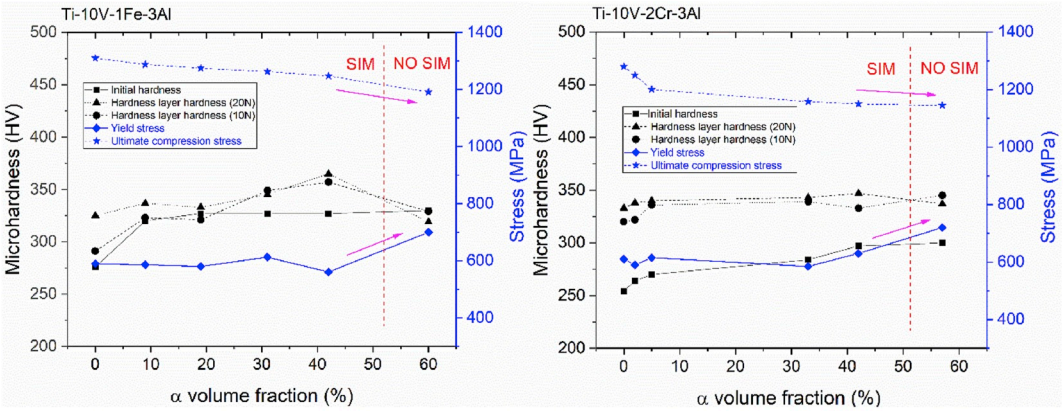

Fig. 10. Various parameters as a function of α volume fraction (a) Ti–10V–1Fe–3Al alloy solution treated in β+(α+β) phase field, (b) Ti–10V–2Cr–3Al alloy solution treated in β+(α+β)phase field.

value that the pre-scratches of large indenter have a certain strengthening effect on the sub-surface layer, but the improvement in Ti–10V–2Cr–3Al alloy is obviously stronger than that in Ti–10V–1Fe–3Al alloy.

3.3. Aging treatment

While the spatial distribution of the α and β phase fractions is determined by the high temperature heat treatment, aging is a suitable method to change the mechanical properties of the phases while keeping the overall microstructural topology unchanged. To create a set of aged microstructures, samples were first solutionised in the β phase field (900 °C for 15 min) and then quenched to room temperature, then reheated to the aging temperature of 400 °C, 550 °C, 700 °C respectively, again soaked for 15 min and subsequently quenched. The optical micrographs for the aging conditions of 400 °C/15min and 550 °C/15 min shown in Fig. 11 are microstructurally identical. For these two alloys, the resulting microstructure shows large β grains in which

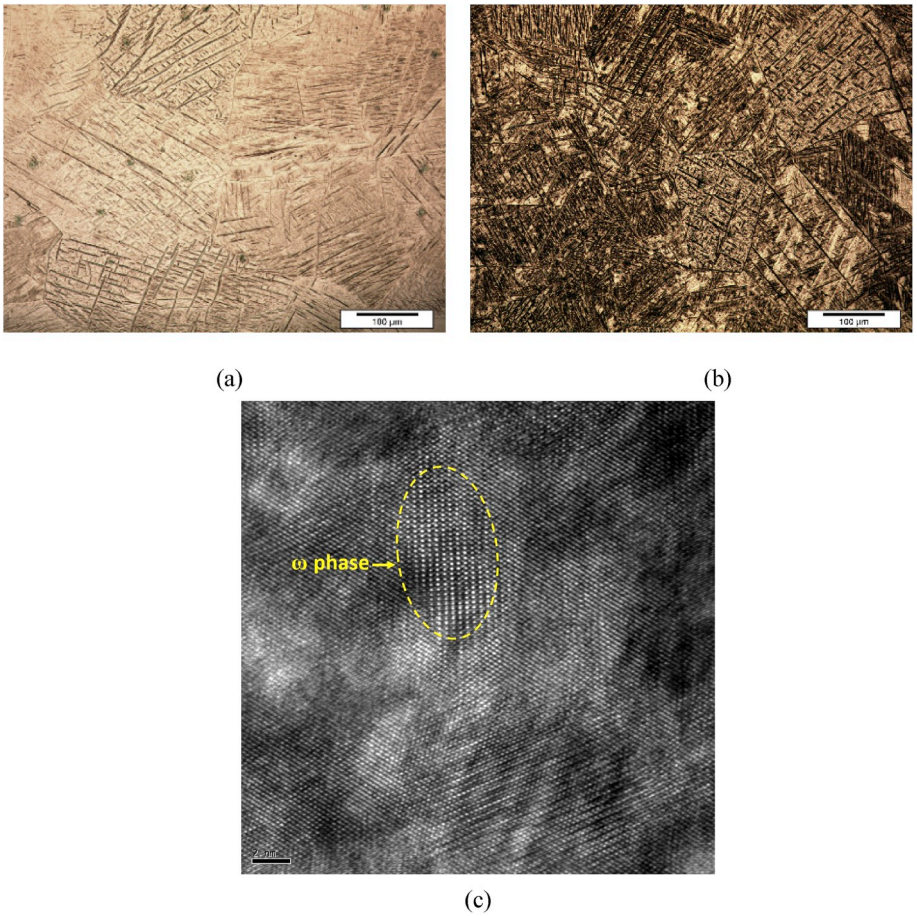

Fig. 11. Typical optical micrographs of the alloys after low temperature aging treatment (a) Ti–10V–1Fe–3Al, (b) Ti–10V–2Cr–3Al, (c) HRTEM image of omega phase in Ti–10V–1Fe–3Al alloy.

acicular shaped martensite had precipitated. The relatively low temperature aging does not change substantially the structure of the alloys quenched from the β region, it still preserves much martensite. A high resolution transmission electron microscopy (HRTEM) image was obtained from these samples, and some nano-ω phase was found, as shown in figure (c).

With the aging temperature increasing to 700 °C, acicular martensite transforms to fine needle shaped α phase, as shown in Fig. 12. The α phase is located both at the prior β grain boundaries and within β grains.

Scratch depth values as a function of the pre-load for alloys having received an aging treatment are shown in Fig. 13. For different aging temperatures, the wear resistance of the two alloys shows different trends in general. At the two lower ageing temperatures the depth of most scratches increases with the preload, indicative of a decreasing abrasion resistances. According to the microstructure observation, a large number of isothermal ω phases is formed in the samples upon aging at low and medium temperatures. This kind of phase is very hard and brittle. The wear resistance of the alloy changes greatly when aging temperature rises to 700 °C. Due to the disappearance of ω phase and the precipitation of aging α phase, the surface hardness of the sample decreases greatly, which makes the scratch value on the initial surface increase greatly. However, when increasing the pre-load, the scratch depth decreases rapidly. When the load is 10 N, the scratch depth value is almost equal to that of the low-temperature aging sample. For Ti–10V–1Fe–3Al samples, when the pre-load increases to 15 N, the alloy enters the transition zone, and the scratch value increases when the load is 20 N. For Ti–10V–2Cr–3Al samples, 10 N is the transition load, and the subsequent increase in pre-load leads to a slight increase in scratch depth. So, while low temperature annealing is beneficial for abrasion resistance at low loads, high temperature annealing is to be preferred when the local loads during the abrasion processes are high.

3.4. Morphology of the groove

Fig. 14 (a)-(b) and (c)-(d) display typical scratch grooves made by the small indenter on the pre-scratch via the large indenter under loads of 0 N, 10 N for Ti–10V–1Fe–3Al alloy with 900 °C/15 min + quenching+550 °C/15 min (NO SIM) and 900 °C/15 min + 700 °C/10 min (SIM) heat treatments, respectively. The pre-scratch with 0 N refers to the scratch produced by the small indenter on the original surface. It should be noted that the scratch tracks in Fig. 12 are grooves created by small indenter, and the whole field of view is located in the central area of the large scratches generated by the large indenter. Fig. 14(a)-(b) depict the damage mechanism of the no-SIM samples. The scratch track on the initial surface (Fig. 14(a)) shows that the failure mechanism is mainly ploughing but there is some debris formation on the edge of the scratch because of the brittle nature and low work hardening capability of the sample. When the pre-scratch load was increased to 10 N, the failure mechanisms did not change too much. Typical scratch grooves of the samples showing SIM are shown in Fig. 14 (c) - (d). Because of the good combination of ductility, strain hardening and strength, all scratch tracks remain smooth without delamination or cracks. As the pre-scratch load increases to 10 N, similar damage mechanism displayed which suggests the surface is completely work hardened after the pre-scratching of the surface with the large indenter. This is really different from the results concluded from the steels whose scratch track morphology is strongly affected by the pre-scratch loading [15,23]. The reason behind such phenomenon still needs further investigation.

3.5. Cross sectional microstructures

In order to clarify the response of material, microstructures of the cross-sections perpendicular to the scratch track were investigated by SEM. Typical results are shown in Fig. 15. Fig. 15(a) and (b) show the worn scar created by only small indenter on the initial surface and work hardening layer by only large indenter respectively. Figure (c) is the worn scar by the small indenter in the centre of the wear track made by the large indenter with a load of 15 N. In all these three cases the material was Ti–10V–2Cr–3Al alloy annealed at 700 °C for 15min. The scratch created by the small indenter is indicated by the arrows line while the boundary of the work hardening layer generated by the large indenter is marked by dashed lines. It can be measured that the scratch depth in figure (c) is less than that in figure (a) giving evidence of the existence of the sub-surface work hardened layer, as shown in figure (b). The microstructure of the subsurface is strongly changed by the pre-scratch, and the shear deformation is inevitably introduced into the material. The distribution of shear deformation degree is not uniform, and it tends to decrease from surface to interior. The figure also shows that the scratch of the small indenter is right in the area of the pre-scratch, which indicates that the scratch depth produced by the small indenter truly reflects the behavior of the work hardening layer. Figure (d) is a work hardening layer with SIM transformation in Ti–10V–1Fe–3Al alloy with 900 °C/15min + 700 °C/7 min, it clear shows that some stress induced martensites are formed and the deformation energy is consumed by the structure transformation.

The variations of the subsurface layer thickness under different pre-loading conditions are shown in Fig. 16. For all samples there is a monotonic increase with the increase of loading applied on the large indenter. However, the slope differs between different alloy grades. In samples with a lower hardness, a thicker work hardening layer is easily formed, while for the low temperature aged specimens, the deformation for a given applied force only lead to a relatively shallow hardening layer.

4. Discussions

Traditionally, scratch tests used to predict the abrasion resistance of metallic materials are carried out on the original fresh surface. The

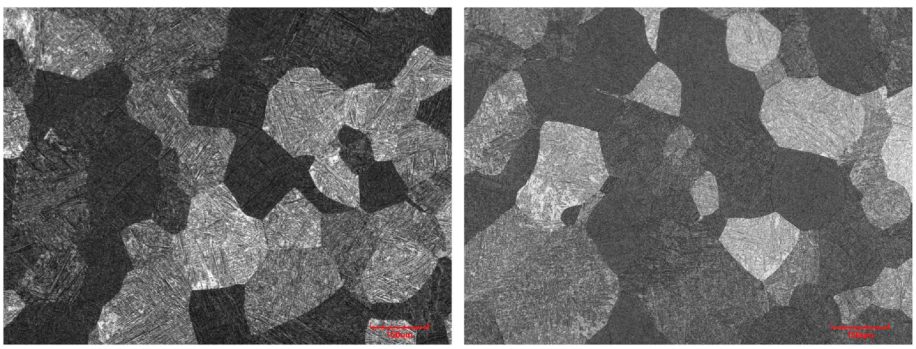

(a) (b)

Fig. 12. Optical micrographs of the alloys after high temperature aging treatment. (a) Ti–10V–1Fe–3Al, (b) Ti–10V–2Cr–3Al (scale bar =160 μm).

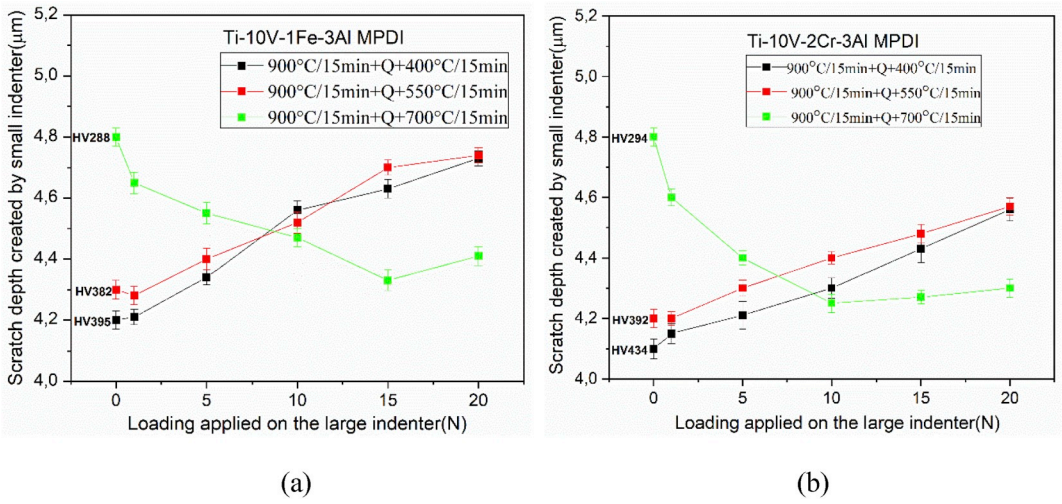

Fig. 13. The scratch depth as a function of the applied load on the large indenter for alloys after aging treatment (a) Ti–10V–1Fe–3Al, (b) Ti–10V–2Cr–3Al.

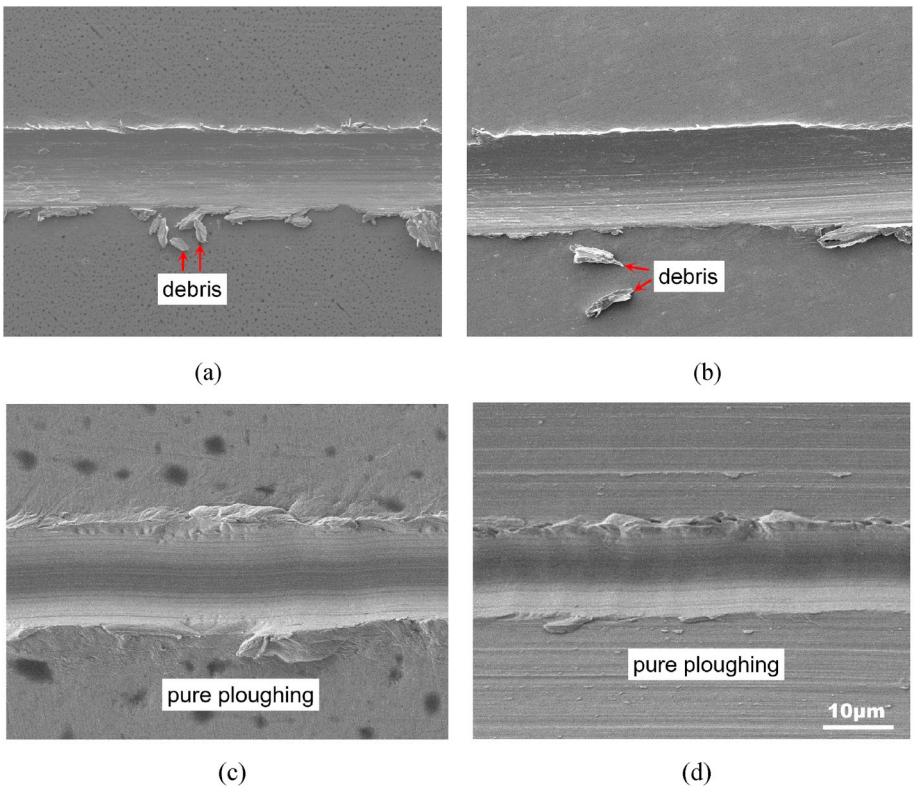

Fig. 14. Scratch tracks of Ti–10V–1Fe–3Al alloy by the small indenter with 0.3 N following pre-scratching under 0 N, 10 N loads (a)-(b): 900 °C/15 min + Q+550 °C/15 min, (c)-(d): 900 °C/15 min + 700 °C/10 min.

MPDI method proposed here involves scratching with a small indenter on the scratch track produced by a larger indenter. Therefore, the current method reflects the work hardening effect of sub-surface layer, which approximates the worn surface formed in the continuous wear process. By studying scratch behaviour under different loading conditions, the abrasion resistance of materials under either mild or harsh conditions can be predicted. The scratch test results show that the wear resistance of the material depends not only on the surface hardness and microstructure of itself, but also on the deformation behaviour and work hardening ability of the material. These factors may change the failure mechanism of materials. In the discussion, the effect of various microstructure and phase transformation (in particular Stress Induced Martensite) on scratch resistance is analysed.

Several distinct microstructures have been created by different heat treatment processes: near-spherical or rod-like α phase was produced by initial state and solid solution treatment in two-phase region, metastable β grains and acicular martensite phase were obtained when the annealing was done at a temperature well within the β phase field, flake α phase or Widmanstätten α phase was produced by β+(α+β) solid solution treatment, fine acicular α phase formed when a high temperature aging treatment was applied, and a high density of nano ω phase precipitates was produced by aging at a low and medium temperatures. Microstructure is one of the key factors in abrasion as it affects how load influences the wear rate, and changes in subsurface microstructure

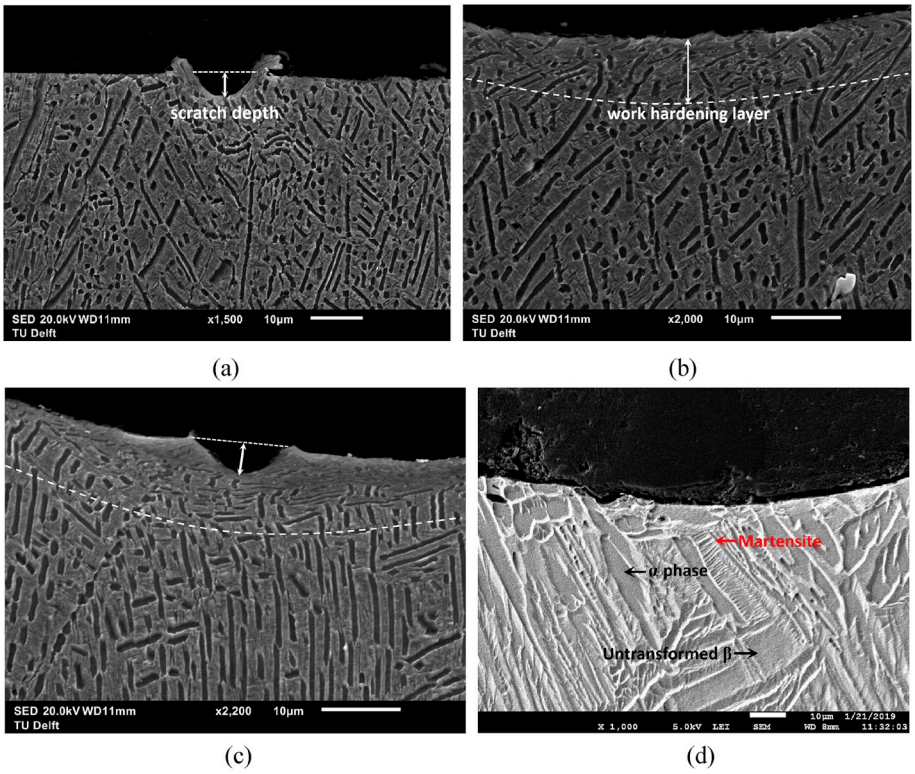

Fig. 15. Microstructure of scratch track in cross-section (a) worn scar by only small indenter, (b) work hardening layer by only large indenter at a load of 15 N, (c) worn scar by the small indenter in the centre of the wear track made by the large indenter with a load of 15 N, (d) work hardening layer with SIM transformation with a load of 5 N.
*Note:(a)~(c) are the images of Ti–10V–2Cr–*3Al *alloy with 700°C/*15 min *treatment, (d) is the images of Ti–10V–1Fe–*3Al *alloy with 900°C/*15min + *700°C/* 7 min.

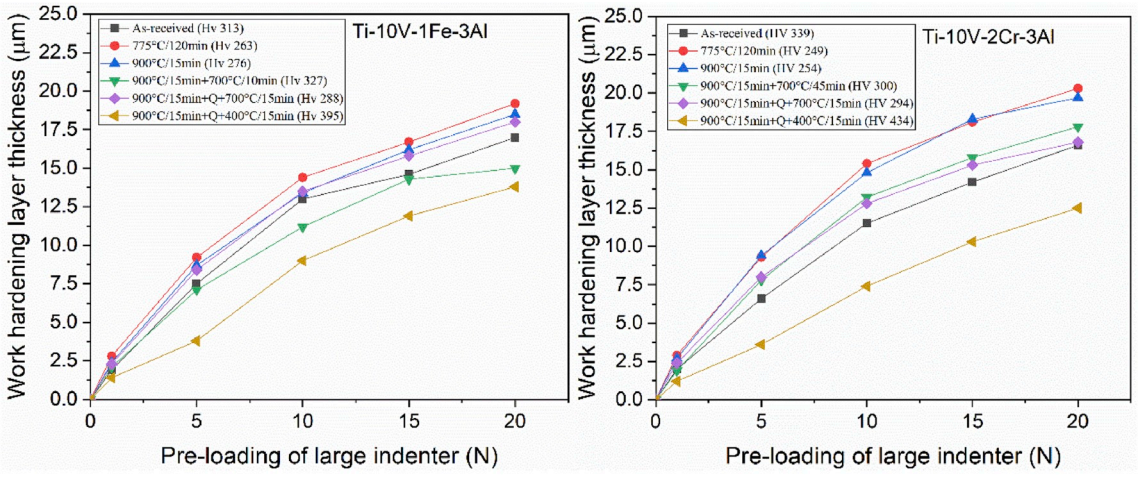

Fig. 16. Work hardening layer thickness as a function of pre-loading of large indenter for (a) Ti–10V–1Fe–3Al, (b) Ti–10V–2Cr–3Al.

influences wear behaviour. The effect of the reinforcing phase depends on the identity, size and the distribution of this phase and also on size and identity of abrasive particles used or more generally on the wear system. When samples are solution treated in the two-phase region, the hardness of the samples decreases with annealing temperature and time, while the ratio of α phase (harder phase) decreases gradually, and the proportion of β phase (softer phase) increases. Therefore, when the pre-load is low, the wear resistance of samples containing a higher α phase fraction is better. With increasing load on the large indenter used to create a controlled wear track, the work hardening of the sub-surface leads to a decrease of the scratch depth. However, if the β phase present is metastable, the stress-induced martensitic transformation of samples having a low initial surface hardness leads to an enhancement of the surface hardening effect and a more obvious decrement of the scratch depth, i.e. a better abrasion resistance. For pre-loads on the large indenter larger than typically 10 N, the scratch depth value of samples with more α phase start to increase, which is indicative of enhanced abrasion losses. In contrast in the samples with enough metastable β phase the scratch depth continued to decrease due to the SIM effect, and this is indicative of a high abrasion resistance. The much reinforced strengthening ability makes the scratch resistance of such alloys under severe loading conditions superior to those of specimens without SIM effect. Comparing these two alloys, it is found that the abrasion resistance of the Ti–10V–2Cr–3Al alloy is more sensitive to the conditions of the α+β solution treatment. The initial static hardness values change a lot as a function of the holding time. For samples heat treated with β or β

+(α+β) solid solution treatment, as opposed to samples treated with α+β solid solution, with the prolongation of holding time in two-phase region, more and more flaked α forms, and the hardness value of these samples also increases. Therefore, for samples in this group, when the pre-load is low, samples with longer solution time have better abrasion resistance. When the pre-load is high, the scratch value of the sample rises again (e.g. 900 °C/15 min + 700 °C/15 min for Ti–10V–1Fe–3Al and 900 °C/15 min + 700 °C/45 min for Ti–10V–2Cr–3Al) because of the excess proportion of α. Only samples with a proper amount of α phase (higher hardness) and metastable β phase (producing SIM effect) have the excellent wear resistance (such as: 900 °C/15 min + 700 °C/7, 10min for Ti–10V–1Fe–3Al and 900 °C/15min + 700 °C/25, 35min for Ti–10V–2Cr–3Al). Similar to the previous research on dual phase steels having different morphologies [23], in titanium alloys a proper mixture of a ductile metastable β phase and a strong flake shaped phase α can improve the scratch resistance, to a level well above that of a harder initial microstructure having the β phase in a stable form. A larger number of hard flake α phase guarantees a good start-up performance on the initial surface, while the metastable β phase enables a SIM transformation resulting in a high degree of work hardening. In low pre-scratch condition, the tough α phase provides an acceptable abrasion resistance, and under high pre-scratch loading, ductile β accommodates the stress and trigger the SIM transformation and simultaneously obtains strain hardening and improves the scratch resistance. The much improved work hardening of dual phase mixture makes the strengthening domain extend to a high pre-scratch load, up to 20 N, as shown in Fig. 9. The plotted data clearly clarifies that a combination of metastable β and flake α in a mixed microstructure could result in a synergistic effect on the scratch resistance. In steels, a calculation based on the conservation of energy lead to the conclusion that some 95% of the energy during abrasive wear is consumed in structural changes at the surface, such as phase transformation, for example that of retained austenite. The improvement in abrasion wear resistance is related to both the hardening effect of the retained austenite and/or the strain induced transformation of austenite into martensite. Such transformation also leads to compressive stresses at the surface which enhances the local ductility and hence permit the wear surface to achieve higher hardness. However, the role of retained austenite on wear resistance is inconclusive as some reports claim improved wear resistance due to work-hardening, while others show harmful or on effect of retained austenite on wear resistance depending on loading conditions [9]. In the present study, from Figs. 6 and 10, it can be concluded that a certain amount of retained austenite (β phase) and SIM transformation could apparently enhance the wear resistance via the mechanical property improvement of the surface or matrix in titanium alloys. The detailed values of starting core hardness, hardness under the large scratch at different loads (10 N and 20 N), compressive yield stress, ultimate compressive strength have also been listed in appendix A (Tables 4 and 5) for Ti–10V–1Fe–3Al and Ti–10V–2Cr–3Al respectively. Coming back to the effect of the chemical composition of the two alloys, it is interesting to reflect on the fact that Ti–10V–1Fe–3Al alloy is more sensitive to the solution treatment of β+(α+β), and the hardness change is greater than that of Ti–10V–2Cr–3Al alloy. Previous transformation kinetics studies [20] on these two alloys have shown that diffusional partitioning of Fe or Cr takes place during the transformation from the β to the α phase. Because the diffusion rate of Fe is higher than that of Cr, the phase transition rate of Ti–10V–1Fe–3Al is much faster than that of Ti–10V–2Cr–3Al alloy. Subsequently, the wear resistance of the former exhibits a higher heat treatment sensitivity. By ageing the two-phase alloys at low or modest temperatures the formation of hard but brittle nano-ω phase precipitates brings excellent wear resistance at low pre-loads, but with the increase of load, its performance deteriorates. Due to the low work hardening ability, the scratch resistance improvement caused by strain hardening is very limited, or even missing. In contrast, the fine acicular α phase precipitated at a high aging temperature leads to more abrasion at low pre-load levels, but the material performance improves significantly under mechanically more demanding abrasion conditions.

Furthermore, a f_{ab} model for abrasive wear was developed by K.H. Zum Gahr [24] on the basis of different interactions between abrasive particles and the wear material. The ratio of microcutting to microploughing or the amount of volume loss to the volume of the wear groove is described by the f_{ab} value. A theoretical model for calculation the f_{ab} value was given in Ref. [25] and results in

$$f_{ab} = 1 - \left(\frac{\phi_{lim}}{\phi_s}\right)^{2/\beta}$$

Where ϕ_s is the effective deformation on the wearing surface and ϕ_{lim} is the capability of deformation of the wearing material during abrasion in a given tribosystem. β is a factor which describes the decay of deformation with increasing depth below the wearing surface and depends mainly on the work-hardening behaviour of the wearing material. Hence the f_{ab} value is not only a material property but it is also a function of the operating conditions during abrasive wear. Our experimental results are highly consistent with this well known model.

Finally, by comparing the wear resistance of all different microstructures of these two alloys, it can be concluded that dual microstructures of a meta-stable β and a flaked α phase, as obtained after an α+(α+β) solid solution treatment have the best wear resistance for a wide range of pre-loading conditions. It is worth mentioning that for higher pre-loads (>20 N), i.e. reflecting very harsh abrasive conditions, the β solid solution treatment may also have a good potential, which deserves further study.

5. Conclusion

In the present study, a novel multi-pass dual-indenter scratch methodology originally developed to measure the abrasion resistance of low alloyed construction steels is applied to investigate the abrasion resistance of two newly developed titanium alloys with different microstructure and work hardening capacity. It is shown that a proper dual phase mixture of a ductile metastable β and a strong flake shaped α phase could be an attractive option to improve the abrasion resistance under demanding conditions, instead of aiming for a microstructure with the highest static hardness via an ageing treatment, which should be optimal for mild abrasive conditions. For the two alloys studied here the best abrasion resistance was obtained after a multistep heat treatment involving annealing in the β phase field immediately followed by annealing in the α+β phase field for the right amount of time.

Declaration of competing interest

We declare that we do not have any commercial or associative interest that represents a conflict of interest in connection with the work submitted.

Acknowledgment

The authors gratefully acknowledge the financial support provided by National Natural Science Foundation of China (Grant No. 51775055), Natural Science Foundation of Hunan Province, China (2018JJ3539, 2019JJ40300), China Scholarship Council(CSC) and Hunan Province 2011 Collaborative Innovation Center of Clean Energy and Smart Grid.

Appendix A

As appendix A.

Table 4
Mechanical properties of heat treated Ti–10V–1Fe–3Al alloy

Heat treatment	Loading	Subsurface hardness (Hv)	Initial hardness (Hv)	Yield stress (MPa)	Compression strength (MPa)
As received	10 N	339	313	1150	1170
	20 N	337			
700 °C/15min	10 N	335	303	950	1100
	20 N	323			
775 °C/15min	10 N	331	272	460	1234
	20 N	345			
775 °C/60min	10 N	329	268	480	1232
	20 N	339			
775 °C/120min	10 N	319	263	465	1290
	20 N	339			
900 °C/15min	10 N	291	276	590	1310
	20 N	325			
900 °C/15min + 700 °C/2min	10 N	323	320	586	1288
	20 N	337			
900 °C/15min + 700 °C/5min	10 N	321	327	580	1275
	20 N	333			
900 °C/15min + 700 °C/7min	10 N	349	327	613	1263
	20 N	345			
900 °C/15min + 700 °C/10min	10 N	357	327	561	1248
	20 N	365			
900 °C/15min + 700 °C/15min	10 N	329	330	700	1191
	20 N	319			
900 °C/15min + Quenching+400 °C/15min	10 N	393	395	1280	1400
	20 N	402			
900 °C/15min + Quenching+550 °C/15min	10 N	385	382	1300	1350
	20 N	391			
900 °C/15min + Quenching+700 °C/15min	10 N	279	288	920	1158
	20 N	291			

Table 5
Mechanical properties of heat treated Ti–10V–2Cr–3Al alloy

Heat treatment	Loading	Subsurface hardness (Hv)	Initial hardness (Hv)	Yield stress (MPa)	Compression strength (MPa)
As received	10 N	353	339	1220	1300
	20 N	324			
700 °C/15min	10 N	333	298	1110	1220
	20 N	330			
775 °C/15min	10 N	320	261	420	1190
	20 N	336			
775 °C/60min	10 N	336	260	420	1180
	20 N	346			
775 °C/120min	10 N	350	249	435	1200
	20 N	341			
900 °C/15min	10 N	320	254	610	1280
	20 N	333			
900 °C/15min + 700 °C/5min	10 N	322	264	590	1250
	20 N	338			
900 °C/15min + 700 °C/15min	10 N	336	270	615	1200
	20 N	340			
900 °C/15min + 700 °C/25min	10 N	339	284	585	1158
	20 N	343			
900 °C/15min + 700 °C/35min	10 N	333	297	630	1150
	20 N	347			
900 °C/15min + 700 °C/45min	10 N	345	300	720	1145
	20 N	337			
900 °C/15min + Quenching+400 °C/15min	10 N	428	434	1250	1390
	20 N	433			
900 °C/15min + Quenching+550 °C/15min	10 N	395	392	1350	1400
	20 N	396			
900 °C/15min + Quenching+700 °C/15min	10 N	345	294	950	1176
	20 N	340			

References

[1] C. Leyens, M. Peters, Titanium and Titanium Alloys-Fundamental and Applications, Wiley-VCH Verlag GmbH&Co. KGaA, Weinheim, Germany, 2003.
[2] F.J. Gil, M.P. Ginebra, J.M. Manero, J.A. Planell, Formation of α-Widmanstätten structure effects of grain size and cooling rate on the Widmanstädtten morphologies and on the mechanical properties in Ti6Al4V alloy, J. Alloy. Comp. 329 (2001) 142–152, https://doi.org/10.1016/S0925-8388(01)01571-7.
[3] F.J. Gil, J.A. Planell, A. Padrós, C. Aparicio, The effect of shot blasting and heat treatment on the fatigue behaviour of titanium for dental implant applications, Dent. Mater. 23 (2007) 486–491, https://doi.org/10.1016/j.dental.2006.03.003.

[4] A. Mishra, Analysis of friction and wear of titanium alloys, Int. J. Mech. Eng. Robot. Res. 3 (2014) 570–573. http://www.ijmerr.com/index.php?m=content&c=index&a=show&catid=124&id=514.
[5] K. Kato, Micro-mechanism of wear - wear modes, Wear 153 (1992) 277–295, https://doi.org/10.1016/0043-1648(92)90274-C.
[6] H. Schimdt, A.S. chminke, M. Schmiedgen, B.B. aretzky, Compound formation and abrasion resistance of ion-implanted Ti6Al4V, Acta Mater. 49 (2001) 487–495, https://doi.org/10.1016/S1359-6454(00)00326-8.
[7] T. Sawase, K. Yoshida, Y. Taira, K. Kamada, M. Atsuta, K. Baba, Abrasion resistance of titanium nitride coatings formed on titanium by ion-beam-assisted deposition, J. Oral Rehabil. 32 (2005) 151–157, https://doi.org/10.1111/j.1365-2842.2004.01382.x.
[8] Y. Zhu, W. Wang, X. Jia, T. Akasaka, S. Liao, F. Watari, Deposition of TiC film on titanium for abrasion resistance implant material by ion-enhanced triode plasma CVD, Appl. Surf. Sci. 262 (2012) 156–158, https://doi.org/10.1016/j.apsusc.2012.03.152.
[9] A.R. Chintha, Metallurgical aspects of steels designed to resist abrasion, and impact-abrasion wear, Mater. Sci. Technol. 35 (2019) 1133–1148, https://doi.org/10.1080/02670836.2019.1615669.
[10] K. Farokhzadeh, A. Edrisy, Transition between mild and severe wear in titanium alloys, Tribol. Int. 94 (2016) 98–111, https://doi.org/10.1016/j.triboint.2015.08.020.
[11] K.H. Zum Gahr, Wear by hard particles, Tribol. Int. 31 (1998) 587–596, https://doi.org/10.1016/S0301-679X(98)00079-6.
[12] L. Wang, Q.Y. Zhang, X.X. Li, X.H. Cui, S.Q. Wang, Dry sliding wear behaviour of Ti–6.5Al–3.5Mo–1.5Zr–0.3Si alloy, Metall. Mater. Trans. A 45A (2014) 2284–2296.
[13] G. Subhash, W. Zhang, Investigation of the overall friction coefficient in single-pass scratch test, Wear 252 (2002) 123–134, https://doi.org/10.1016/S0043-1648(01)00852-3.
[14] A. Vencl, N. Manic, V. Popovic, M. Mrdak, Possibility of the abrasive wear resistance determination with scratch tester, Tribol. Lett. 37 (2010) 591–604, https://doi.org/10.1007/s11249-009-9556-x.
[15] X. Xu, S. van der Zwaag, W. Xu, Prediction of the abrasion resistance of constrction steel on the basis of the subsurface deformation layer in a multi-pass dual-indenter scratch test, Wear 338–339 (2015) 47–53, https://doi.org/10.1016/j.wear.2015.05.012.
[16] I.P. Semenova, R.R. Valiev, K.S. Selivanov, Y.M. Modina, A.V. Polyakov, M. K. Smyslova, R.Z. Valiev, Enhanced strength and scratch resistance of ultra-fine grained Ti64 alloy with (Ti+V)N coating, Rev. Adv. Mater. Sci. 48 (2017) 62–70. http://www.ipme.ru/e-journals/RAMS/no_14817/05_14817_valiev.pdf.
[17] K. Holmberg, A. Laukkanen, H. Ronkainen, J. Li, W. Beres, Three-dimensional finite element modelling of the scratch test for a TiN coated titanium alloy substrate, Wear 260 (2006) 1232–1242, https://doi.org/10.1016/j.wear.2005.08.008.
[18] X. Xu, S. van der Zwaag, W. Xu, A novel multi-pass dual-indenter scratch test to unravel abrasion damage formation in construction steels, Wear 322–323 (2015) 51–60, https://doi.org/10.1016/j.wear.2014.10.011.
[19] C. Li, X. Wu, J.H. Chen, S. van de Zwaag, Influence of α morphology and volume fraction on the stress-induced martenstitic transformation in Ti-10V-2Fe-3Al, Mater. Sci. Eng. A 528 (2011) 5854–5860, https://doi.org/10.1016/j.msea.2011.03.107.
[20] C. Li, J. Chen, X. Wu, W. Wang, S. van der Zwaag, Tuning the stress induced martensitic formation in titanium alloys by alloy design, J. Mater. Sci. 47 (2012) 4093–4100, https://doi.org/10.1007/s10853-012-6263-z.
[21] C. Li, J. Chen, Y.J. Ren, W. Li, J.J. He, J.H. Chen, Effect of solution heat treatment on the stress-induced martensite transformation in two new titanium alloys, J. Alloy. Comp. 641 (2015) 192–200, https://doi.org/10.1016/j.jallcom.2015.04.070.
[22] C. Li, J.H. Chen, X. Wu, S. van der Zwaag, A comparative study of the microstructure and mechanical properties of α+β titanium alloys, Met. Sci. Heat Treat. 56 (2014) 374–380, https://doi.org/10.1007/s11041-014-9765-2.
[23] X. Xu, S. van der Zwaag, W. Xu, The effect of ferrite-martensite morphology on the scratch and abrasive wear behavior of a dual phase construction steel, Wear 348–349 (2016) 148–157, https://doi.org/10.1016/j.wear.2015.12.005.
[24] K.H. Zum Gahr, Formation of wear debris by the abrasion of ductile metals, Wear 74 (1981) 353–373, https://doi.org/10.1016/0043-1648(81)90173-3.
[25] K.H. Zum Gahr, Modelling of two-body abrasive wear, Wear 124 (1988) 87–103, https://doi.org/10.1016/0043-1648(88)90236-0.